Conducting Membranes

Deutsche Ausgabe: DOI: 10.1002/ange.201411963
Internationale Ausgabe: DOI: 10.1002/anie.201411963

A Mixed Ionic and Electronic Conducting Dual-Phase Membrane with High Oxygen Permeability**

Wei Fang, Fangyi Liang, Zhengwen Cao, Frank Steinbach, and Armin Feldhoff*

Abstract: *To combine good chemical stability and high oxygen permeability, a mixed ionic-electronic conducting (MIEC) 75 wt% $Ce_{0.85}Gd_{0.1}Cu_{0.05}O_{2-\delta}$-25 wt% $La_{0.6}Ca_{0.4}FeO_{3-\delta}$ (CGCO-LCF) dual-phase membrane based on a MIEC–MIEC composite has been developed. Copper doping into $Ce_{0.9}Gd_{0.1}O_{2-\delta}$ (CGO) oxide enhances both ionic and electronic conductivity, which then leads to a change from ionic conduction to mixed conduction at elevated temperatures. For the first time we demonstrate that an intergranular film with 2–10 nm thickness containing Ce, Ca, Gd, La, and Fe has been formed between the CGCO grains in the CGCO-LCF one-pot dual-phase membrane. A high oxygen permeation flux of 0.70 mL min^{-1} cm^{-2} is obtained by the CGCO-LCF one-pot dual-phase membrane with 0.5 mm thickness at 950 °C using pure CO_2 as the sweep gas, and the membrane shows excellent stability in the presence of CO_2 even at lower temperatures (800 °C) during long-term operation.*

Mixed ionic–electronic conducting (MIEC) oxides are promising candidate materials for catalysts,[1] electrodes of batteries and fuel cells,[2] and also oxygen-transporting membranes (OTMs).[3] OTMs have gained increasing attention owing to their potential applications in oxygen supply,[4] CO_2 capture integrated in oxy-fuel power plants,[5] and catalytic membrane reactors.[6] Most of the well-established MIEC materials for OTMs are oxygen-deficient perovskite oxides, for example, $Ba_{0.5}Sr_{0.5}Co_{0.8}Fe_{0.2}O_{3-\delta}$[7] and $La_{1-x}Sr_xCo_{1-y}Fe_yO_{3-\delta}$.[8] Unfortunately, these perovskites degrade rapidly in the presence of CO_2, H_2O, and other reactive gases,[9] and accordingly their use is rather limited. Although Ca-containing perovskites (for example, $La_{1-x}Ca_xFeO_{3-\delta}$) show great tolerance to CO_2,[10] the oxygen flux is relatively poor and thus it is not desired for practical applications.

Alternatively, fluorite-type CeO_2-based oxides are especially attractive owing to a combination of fast oxygen-ion mobility, good redox catalytic properties, and excellent chemical compatibility with CO_2 and H_2O at elevated temperatures.[11] Furthermore, these materials exhibit n-type electronic conductivity under reducing conditions that is due to a small-polaron hopping process between cerium sites.[12] To improve CeO_2-based oxides with high oxygen-ion conductivity, aliovalent doping with lanthanide cations have been extensively investigated, and the highest ionic conductivities are reported in Gd- and Sm-doped cerias.[12] The conductivities of such cerias are found to be predominantly ionic under oxidizing atmospheres.[12] Many efforts are underway to improve the properties of these oxides further by co-doping techniques.[13] Transition metal oxides such as CuO, Co_3O_4, and MnO_2 have been proposed to improve the sintering behavior and densification of cerias.[14] However, the effect of co-doping of lanthanide and multivalent cations in the CeO_2 structure has not attracted much attention.[15,16] The co-doping behavior increases the ionic conductivity, and also develops the p-type electronic conductivity, which allows the extension of the mixed ionic–electronic conduction to higher oxygen partial pressures (10^{-5} to 10^{-1} atm), but the oxygen permeation of these materials may still be limited by insufficient electronic conductivity.[16,17]

Besides single-phase membranes, dual-phase membranes could be also developed by the combination of ionic conducting (IC) materials and electronic conducting (EC) materials.[18,19] The oxygen transport processes in two conventional concepts for dual-phase membranes are illustrated in Figure 1 a and Figure 1 b, respectively. For an IC–EC composite conductor, it is comprised of a fluorite-type IC oxide (for example, $Ce_{0.9}Gd_{0.1}O_{2-\delta}$, CGO) for oxygen ionic transport and a pure EC oxide ($La_{0.7}Sr_{0.3}MnO_{3-\delta}$) for electronic transport,[18] and the oxygen surface-exchange reaction (OSER) is generally thought to be confined at the triple phase boundary (TPB; Figure 1 a).[20] One strategy to improve the performance has been to replace the pure EC oxide with a perovskite predominantly electronic MIEC oxide ($La_{0.6}Sr_{0.4}Co_{0.2}Fe_{0.8}O_{3-\delta}$) for both oxygen ionic and electronic transport (Figure 1 b).[21] By introducing ionic transport to the EC phase, OSER could take place not only at the TPBs, but also over a significant portion of the MIEC surface, thereby extending the size of the active region and improving the kinetics at high temperatures (800–1000 °C; Figure 1 b).[20] Recently, a MIEC-EC composite membrane ($Ce_{0.8}Tb_{0.2}O_{2-\delta}$-$NiFe_2O_4$) has been also reported.[22] However, the application of these dual-phase materials is still limited owing to low oxygen permeability.

Herein, we report a novel concept of dual-phase membrane, 75 wt% $Ce_{0.85}Gd_{0.1}Cu_{0.05}O_{2-\delta}$ (CGCO)–25 wt% $La_{0.6}Ca_{0.4}FeO_{3-\delta}$ (LCF), comprising of a predominantly ionic MIEC oxide CGCO with a fluorite structure and a predominantly electronic MIEC oxide LCF with a perovskite struc-

[*] W. Fang, Dr. F. Y. Liang, Dr. Z. W. Cao, F. Steinbach, Prof. Dr. A. Feldhoff
Institute of Physical Chemistry and Electrochemistry
Leibniz University Hannover
Callinstrasse 22, 30167 Hannover (Germany)
E-mail: wei.fang@pci.uni-hannover.de

[**] This work has been supported by German Research Foundation (DFG) (no. FE928/7-1). We also acknowledge Y. Y. Wei, A. Schulz, B. Geppert, A. Düvel, and O. Ravkina for technical support.

Supporting information for this article is available on the WWW under http://dx.doi.org/10.1002/anie.201411963.

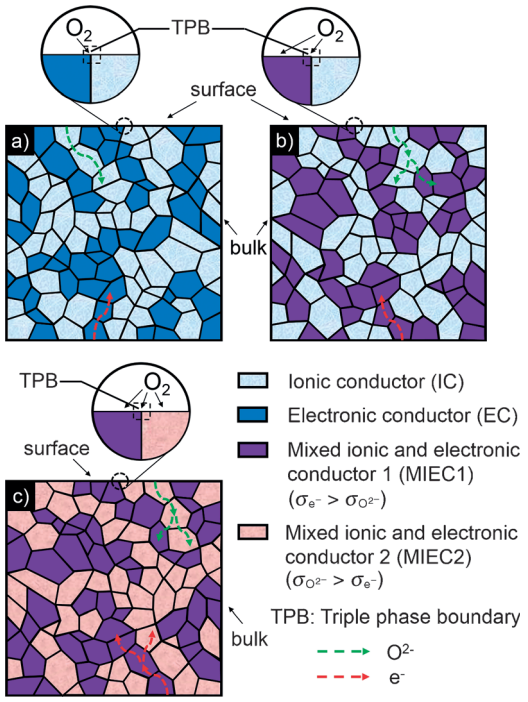

Figure 1. Concept of dual-phase membranes. a) IC–EC conductor. b) IC–MIEC1 conductor. c) MIEC1–MIEC2 conductor. $\sigma_{O^{2-}}$: oxygen ionic conductivity, σ_{e^-}: electronic conductivity.

ture. As illustrated in Figure 1c, with this composite strategy, the oxygen ions and electrons are transported in both MIEC phases at the same time, which enables the OSER to be extended to the overall surface area of the dual-phase membrane, thus significantly increasing the rate of OSER and bulk diffusion for oxygen permeation. This CGCO-LCF dual-phase membrane demonstrates considerable oxygen permeability and excellent stability in the presence of CO_2, exhibiting great potential as competitive OTM.

The dual-phase membranes were prepared by using the powder mixing and one-pot method. X-ray diffraction patterns (Supporting Information, Figure S1) of the as-synthesized powders of these membranes clearly show that both the CGO and CGCO powders consist of a major cubic fluorite phase with space group $Fm\bar{3}m$, while the LCF powder exhibits an orthorhombic perovskite structure with space group *Pnma*. Compared to CGO powders ($a = 541.8$ pm), a slight decrease in lattice parameters was found for CGCO ($a = 541.6$ pm) at room temperature in air, since the radius of Cu^{2+} (73 pm) is smaller than that of Ce^{4+} (97 pm).[23] And CGCO has larger thermal expansion coefficient (TEC) of cell parameters than CGO in air and N_2 atmospheres (Supporting Information, Figure S2 and Table S2). Moreover, it is noticed that the copper doping for the ceria-based oxide enables a substantial improvement of the total conductivity (determined by ionic conductivity) and ambipolar conductivity (determined by the rate limiting steps; Supporting Information, Figures S3–S5). In situ XRD was used to characterize the phase stability of the CGCO-LCF dual-phase materials in air and pure CO_2. The CGCO phase remains unchanged with an increase in the temperature, while the LCF phase reveals a reversible change form orthorhombic to cubic perovskite structure above 700 °C (Supporting Information, Figure S6 and Table S3), and no carbonate formation could be detected over the whole temperature range (Supporting Information, Figure S7).

The surface morphologies of the sintered dual-phase membranes are shown in Figure 2. In comparison to powder

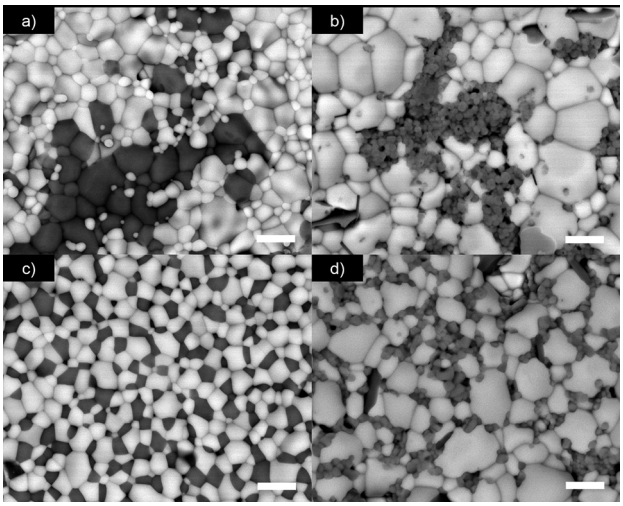

Figure 2. BSE micrographs of the surface of the dual-phase membranes. a) CGO-LCF mix membrane. b) CGCO-LCF mix membrane. c) CGO-LCF one-pot membrane. d) CGCO-LCF one-pot membrane. The light grains are the CGO or CGCO phase, and the dark grains are the LCF phase. Scale bars: 3 μm.

mixing membranes (Figure 2a,b), the membranes prepared by the one-pot method exhibit a much higher homogenization of the two phases (Figure 2c,d). The grains could be distinguished in the back-scattered electron (BSE) micrographs. The BSE micrographs also indicate that Cu-doped CGO has a much larger grain size than CGO. Therefore, we think that copper acts as a sintering aid and significantly lowers the densification temperature. The information about the elemental distribution is confirmed by the energy-dispersive X-ray spectroscopy (EDXS) images of the CGCO-LCF one-pot dual-phase membrane (Supporting Information, Figure S8,S9).

Figure 3 displays the investigation by transmission electron microscopy (TEM) of the CGCO-LCF one-pot dual-phase membrane. An intergranular film between two CGCO grains with the thickness from 2 to 10 nm can be seen by bright contrast in the TEM dark-field micrograph of Figure 3a and by dark contrast in the STEM annular dark-field micrograph of Figure 3b. Electron energy-loss (EEL) spectra as shown in Figure 3c reveal the chemical nature of the CGCO grains and the intergranular film. The three background-substracted EEL spectra were obtained from linescan across the grain boundary between two CGCO grains (Supporting Information, Figure S11). The diameter of the electron beam was 1.5 nm. The spectra for CGCO were taken in ca. 6–8 nm distance to the grain boundary from both sides. The spectra for the two CGCO grains are almost identical and

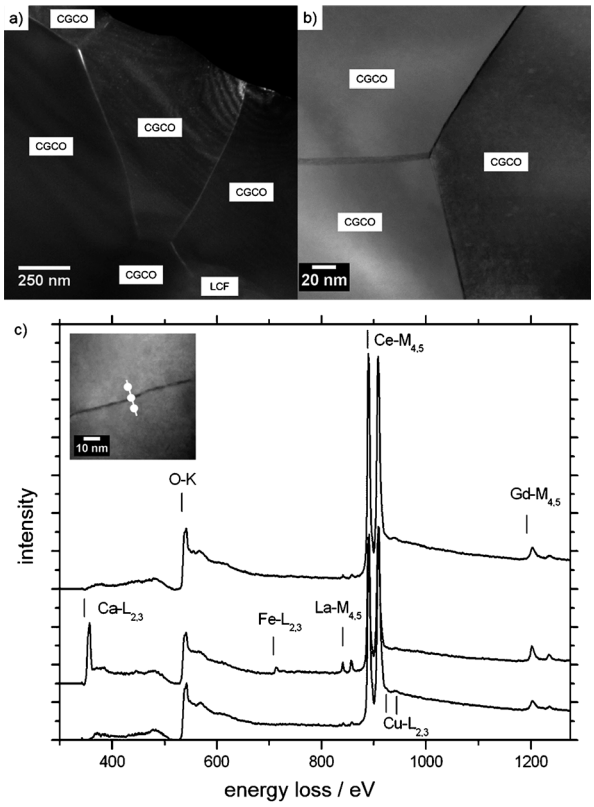

Figure 3. CGCO-LCF one-pot dual-phase membrane. a) TEM dark-field, b) STEM annular dark-field, c) EEL spectra across the grain boundary between two CGCO grains (see inset). Background was subtracted according to power law with supporting points in front of Ca-$L_{2,3}$ edge and in front of the O-K edge. For the full line profile, see the Supporting Information, Figure S11.

show a O-K ionization edge at 534 eV as well as intense Ce-$M_{4,5}$ white lines at 884 eV and weaker Gd-$M_{4,5}$ white lines at 1186 eV. Note the weak white lines of Cu-$L_{2,3}$ at 931 eV can be found, at the right of Ce-$M_{4,5}$ white lines at 884 eV, and La-$M_{4,5}$ white lines at 832 eV. In the spectrum taken from the grain boundary region, these features of the adjacent CGCO grains are present as well, but it also shows a Ca-$L_{2,3}$ ionization edge at 347 eV and a Fe-$L_{2,3}$ ionization edge at 710 eV. It is also observed that at the grain boundary the La-$M_{4,5}$ white line at 832 eV is more intense, but the Cu-$L_{2,3}$ white lines at 931 eV are hard to observe. Therefore, we can conclude that most of Cu is incorporated into the ceria lattice, and no significant segregation of Cu could be found at the grain boundary. One possible explanation for the formation of the intergranular film is that during the one-pot synthesis,[24] a small amount of Ca, La, and Fe can easily segregate at the grain boundary between CGCO grains. A similar effect of CaO addition to CGO was also reported, which had been proved to bring out a positive influence on the grain-boundary conduction.[25] Furthermore, an interdiffusion zone at the interface between the CGCO and LCF grains has been observed by the EEL spectra technique (Supporting Information, Figure S12).

Figure 4 presents the oxygen permeation fluxes of CeO_2-based dual-phase membranes and LCF single-phase membrane as a function of temperature using pure He or CO_2 as the sweep gas. The dual-phase membranes prepared by the one-pot method have better performances than those prepared by powder mixing. This result clearly indicates that the uniformity of grain distribution for the dual-phase membrane is beneficial to improve the oxygen fluxes.[5] Moreover, with our novel MIEC-MIEC composite strategy, the CGCO-LCF one-pot dual-phase membrane exhibits the highest oxygen permeability, while for the traditional CGO-LCF dual-phase membranes, the oxygen permeation fluxes are even slightly lower than that of the LCF single-phase membrane. The highest oxygen permeation fluxes of 0.87 and 0.70 $mL\,min^{-1}\,cm^{-2}$ were obtained at 950 °C with pure He and CO_2 as the sweep gases, respectively. When pure CO_2 was taken as the sweep gas, the oxygen permeation fluxes were slightly decreased because of the inhibiting effect of CO_2 on the OSER.[5]

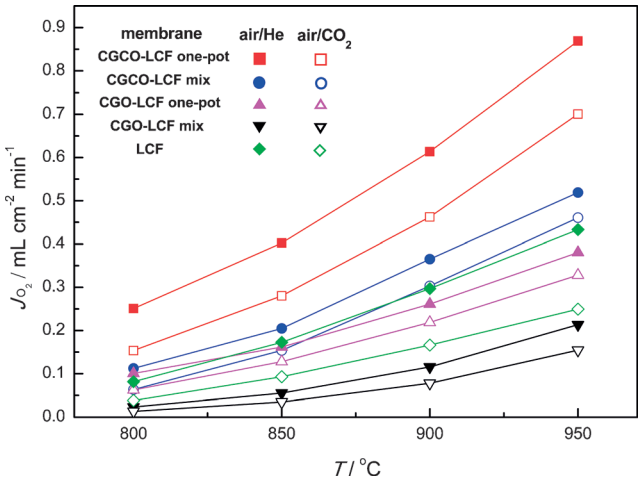

Figure 4. Oxygen permeation fluxes of CeO_2-based dual-phase membranes and the LCF single-phase membrane as a function of temperature. Condition: 100 $mL\,min^{-1}$ air as the feed gas, 30 $mL\,min^{-1}$ He or CO_2 as the sweep gas; membrane thickness: 0.5 mm.

Figure 5 shows the long-term oxygen permeation operation of CGCO-LCF one-pot dual-phase membrane at 800 °C and 900 °C. No decrease of the oxygen permeation fluxes was found during the test, thus indicating that the membrane is CO_2-stable.

In conclusion, for the first time we report an approach to obtain high and stable oxygen permeability of a novel dual-phase membrane. We also demonstrated stable oxygen permeation fluxes of the membrane in a CO_2 atmosphere even at lower-temperature (800 °C) operation. As the oxygen permeability of the membrane can be further improved by reducing the membrane thickness, such as fabricating hollow fibers,[26] or coating MIEC materials on the membrane surface for the enlargement of OSER,[21] it is therefore reasonable to foresee that our CGCO-LCF dual-phase membrane provides promising potential for practical applications.

Keywords: carbon dioxide · electronic conductors · ionic conductors · membranes · oxygen transport

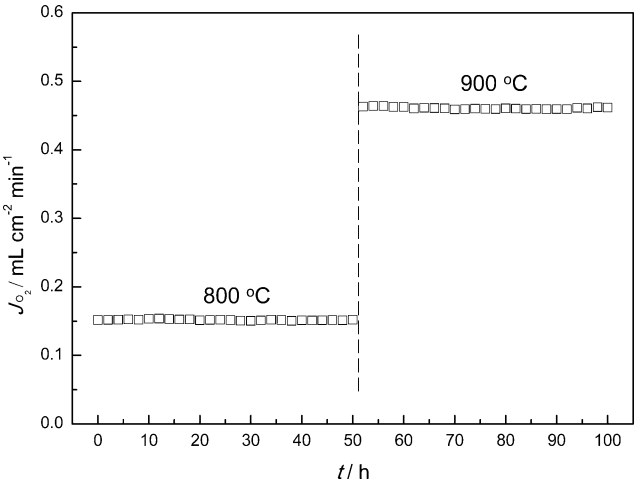

Figure 5. Long-term oxygen permeation operation through the CGCO-LCF one-pot dual-phase membrane. Conditions: 100 mL min^{-1} air as the feed gas, 30 mL min^{-1} CO_2 as the sweep gas, membrane thickness: 0.5 mm.

How to cite: *Angew. Chem. Int. Ed.* **2015**, *54*, 4847–4850
Angew. Chem. **2015**, *127*, 4929–4932

[1] A. Aguadero, H. Falcon, J. M. C. Martin, S. M. A. Zahrani, J. L. G. Fierro, J. A. Alonso, *Angew. Chem. Int. Ed.* **2011**, *50*, 6557–6561; *Angew. Chem.* **2011**, *123*, 6687–6691.
[2] J. Suntivich, H. A. Gasteiger, N. Yabuuchi, H. Nakanishi, J. B. Goodenough, Y. S. Horn, *Nat. Chem.* **2011**, *3*, 546–550.
[3] Y. Liu, X. F. Zhu, M. R. Li, H. Y. Liu, Y. Cong, W. S. Yang, *Angew. Chem. Int. Ed.* **2013**, *52*, 3232–3236; *Angew. Chem.* **2013**, *125*, 3314–3318.
[4] H. H. Wang, S. Werth, T. Schiestel, J. Caro, *Angew. Chem. Int. Ed.* **2005**, *44*, 6906–6909; *Angew. Chem.* **2005**, *117*, 7066–7069.
[5] H. X. Luo, K. Efimov, H. Q. Jiang, A. Feldhoff, H. H. Wang, J. Caro, *Angew. Chem. Int. Ed.* **2011**, *50*, 759–763; *Angew. Chem.* **2011**, *123*, 785–789.
[6] Z. W. Cao, H. Q. Jiang, H. X. Luo, S. Baumann, W. A. Meulenberg, J. Assmann, L. Mleczko, Y. Liu, J. Caro, *Angew. Chem. Int. Ed.* **2013**, *52*, 13794–13797; *Angew. Chem.* **2013**, *125*, 14039–14042.
[7] Z. P. Shao, W. S. Yang, Y. Cong, H. Dong, J. H. Tong, G. X. Xiong, *J. Membr. Sci.* **2000**, *172*, 177–183.
[8] Y. Teraoka, Y. Honbe, J. Ishii, H. Furukawa, I. Moriguchi, *Solid State Ionics* **2002**, *152–153*, 681–687.
[9] Y. J. X. Yi, S. J. Feng, Y. B. Zuo, W. Liu, C. S. Chen, *Chem. Mater.* **2005**, *17*, 5856–5861.
[10] K. Efimov, T. Klande, N. Juditzki, A. Feldhoff, *J. Membr. Sci.* **2012**, *389*, 205–215.
[11] K. Schmale, M. Grünebaum, M. Janssen, S. Baumann, F. S. Küppers, H. D. Wiemhöfer, *Phys. Status Solidi B* **2011**, *248*, 314–322.
[12] M. Mogensen, N. M. Sammes, G. A. Tompsett, *Solid State Ionics* **2000**, *129*, 63–94.
[13] S. Banerjee, P. S. Devi, D. Topwal, S. Mandal, K. Menon, *Adv. Funct. Mater.* **2007**, *17*, 2847–2854.
[14] C. Kleinlogel, L. J. Gauckler, *Adv. Mater.* **2001**, *13*, 1081–1085.
[15] G. S. Lewis, A. Atkinson, B. C. H. Steele, J. Drennan, *Solid State Ionics* **2002**, *152–153*, 567–573.
[16] S. Lübke, H. D. Wiemhöfer, *Solid State Ionics* **1999**, *117*, 229–243.
[17] M. Balaguer, C. Solís, J. M. Serra, *Chem. Mater.* **2011**, *23*, 2333–2343.
[18] V. V. Kharton, A. V. Kovalevsky, A. P. Viskup, F. M. Figueiredo, A. A. Yaremchenko, E. N. Naumovich, F. M. B. Marques, *J. Electrochem. Soc.* **2000**, *147*, 2814–2821.
[19] V. V. Kharton, A. V. Kovalevsky, A. P. Viskup, A. L. Shaula, F. M. Figueiredo, E. N. Naumovich, F. M. B. Marques, *Solid State Ionics* **2003**, *160*, 247–258.
[20] S. B. Adler, *Chem. Rev.* **2004**, *104*, 4791–4843.
[21] J. H. Joo, K. S. Yun, Y. Lee, J. Jung, C. Y. Yoo, J. H. Yu, *Chem. Mater.* **2014**, *26*, 4387–4394.
[22] M. Balaguer, J. G. Fayos, C. Solís, J. M. Serra, *Chem. Mater.* **2013**, *25*, 4986–4993.
[23] R. D. Shannon, *Acta Crystallogr.* **1976**, *32*, 751–767.
[24] X. F. Zhu, H. H. Wang, W. S. Yang, *J. Membr. Sci.* **2008**, *309*, 120–127.
[25] P. S. Cho, S. B. Lee, Y. H. Cho, D. Y. Kim, H. M. Park, J. H. Lee, *J. Power Sources* **2008**, *183*, 518–523.
[26] S. M. Liu, G. R. Gavalas, *J. Membr. Sci.* **2005**, *246*, 103–108.

Received: December 12, 2014
Published online: February 23, 2015

